NRIAG JOURNAL OF ASTRONOMY AND GEOPHYSICS
2019, VOL. 8, NO. 1, 45–54
https://doi.org/10.1080/20909977.2019.1617559

Utility of GNSS Radio Occultation technique for tropopause height investigation over Egypt

Mohamed Zhran[a], Ashraf Mousa[b], Mostafa Rabah[c] and Zaki Zeidan[a]

[a]Public Works Engineering Department, Faculty of Engineering, Mansoura University, El-Mansoura, Egypt; [b]National Research Institute of Astronomy and Geophysics, Helwan, Egypt; [c]Benha Faculty of Engineering, Benha University, Egypt

ABSTRACT

Global Navigation Satellite System (GNSS) Radio Occultation (RO) is an active limb sounding technique, where GNSS satellites transmitted signals passing through the atmosphere of the Earth and received by a GNSS receiver on low earth orbiter (LEO) satellite. RO provides accurate atmospheric refractivity profile. RO technique has been widely used to study the atmosphere of planets. This paper investigates the use of GNSS RO for tropopause height (TPH) estimation as one of the key climate parameters over Egypt. TPH is also very important in determining the wet delay in GNSS analysis. Two years (2016 and 2017) of MetOP A and B satellites data are used. ROPP software package is used in the analysis. For validation of the results, RO-derived TPH is compared with European Centre for Medium-Range Weather Forecast (ECMWF) model as well as radiosonde (RS). Good agreement and high correlation are found between TPH from RO and ECMWF and RS on the other hand. TPH varies between 14 and 16 km over Egypt. It decreases with latitude and shows no clear trend with longitude. Tropopause temperature is found to increase with latitude.

KEYWORDS

GNSS Radio Occultation; tropopause height; lapse rate; tropopause temperature; radiosonde; ECMWF model; WMO

1. Introduction

Global Navigation Satellite System (GNSS) Radio Occultation (RO) technique is one of the most important meteorological applications of GNSS. This study focuses on the application of GNSS RO in atmospheric observation technique to calculate tropopause height (TPH) for Egypt. TPH is a very important parameter for weather and atmospheric phenomena. Studying the tropopause structure necessitate detailed vertical atmospheric profile information (Fueglistaler et al. 2009; Randel et al. 2007; Holton et al. 1995).

GNSS RO technique derives atmospheric profiles with a high vertical resolution and makes the spatial distribution of the data more homogenous (Fu 2011). Atmospheric profiles coming from GNSS RO are not affected by geographic areas as compared to radiosonde (RS). Generally, RS data have vertical resolution ranging from a few hundred metres to about a kilometre, and this is also considered as a limitation for tropopause.

Throughout this paper, ROPP V.9 is used to process the measurement data for the RO. This research gives details of TPH distribution over Egypt. This includes investigating the spatial and temporal variations of TPH. It is found that TPH varies between 14 and 16 km. Generally, TPH decreases with latitude while no clear relation is found between TPH and longitude.

2. GNSS radio occultation concept

GNSS RO is a relatively new remote sensing technique for exploring the atmosphere of the Earth (Kursinski et al. 1997; Hajj et al. 2002). It delivers key properties of the free atmosphere, such as pressure and temperature. RO measurements are based on radio signals emitted by GNSS satellites (Anthes 2011; Steiner et al. 2011). The rays are refracted by the atmosphere of the Earth and are received by a LEO satellite in a limb-sounding geometry (Figure 1).

GNSS RO for investigating the atmosphere of the Earth was first proposed for the NASA Earth Observing System and demonstrated successfully in 1995, when measurements by a GPS receiver onboard GPS/MET confirmed the potential of the technique (Ware et al. 1996; Kursinski et al. 1997). GNSS RO has since then emerged as remote sensing technique for the atmosphere of the Earth that is relatively inexpensive, has high precision, accuracy, long-term stability, all-weather-capability and high vertical resolution. These properties also indicate the general suitability of RO for climate applications (Anthes et al. 2008; Steiner et al. 2011).

Bouguer's formula (Born and Wolf. 1999), which represents the equation for the ray trajectory in a spherically symmetrical refractive field, and replaces Snell's law for a plane stratified medium:

CONTACT Mohamed Zhran zhran_eng@yahoo.com Public Works Engineering Department, Faculty of Engineering, Mansoura University, Al Mansurah, Egypt

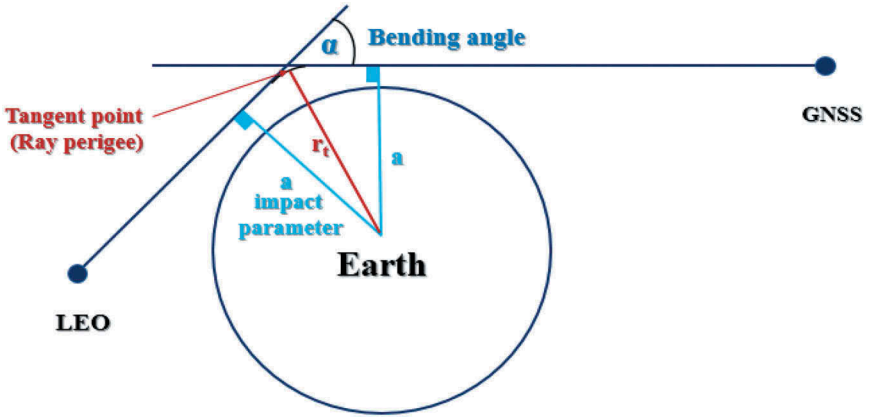

Figure 1. Geometry of GNSS – LEO satellite occultation.

$$nr\sin\phi = const = a \tag{1}$$

The quantity $rsin\phi$ represents the perpendicular distance from the origin to the ray path tangent. As r goes to infinity (straight line), n goes to unity, so that the constant term in the previous formula must equal the impact parameter (a). Generally, ϕ is the angle between the radius vector and the ray path and in Figure 1, ϕ equals 90° at the tangent point so $sin\phi = 1$ (unity) and this leads to $a = n\ (r_t)\ r_t = n\ r_t$. Where r_t is the tangent point radius, which represents the distance between the centre of curvature and the tangent point as defined in Figure 1. Ontheotherhand a is the so-called impact parameter that is defined with range units and constant along a ray trajectory.

In RO, the change of that quantity, i.e. $\frac{dL}{dt}$ in ms^{-1} or the Doppler shift $f_D$in Hz is the key observable (e.g. Kirchengast et al. 2006):

$$f_D = -\frac{f}{c}\frac{dL}{dt} \tag{2}$$

Where:

f_D: denotes the excess Doppler shift on the carrier frequencies f_i caused by the neutral atmosphere and the ionosphere.
c: is the light speed in vacuum.
t: is time.

The signals $L1$ and $L2$ travel on different paths because ionospheric bending depends on the frequency. A linear combination leads to the removing of the first-order ionospheric effect:

$$\Delta L_c = \frac{f_1^2\Delta L_1 - f_2^2\Delta L_2}{f_1^2 - f_2^2} \tag{3}$$

ΔL_c contains the neutral atmosphere particular fractions (Foelsche 1999). Vorob'ev and Krasil'nikova (1994) suggested to use the combination of the two bending angles (α_1 and α_2) at the same impact factors:

$$\alpha_c(a) = \frac{f_1^2\alpha_1(a) - f_2^2\alpha_2(a)}{f_1^2 - f_2^2} \tag{4}$$

$\alpha_1(a)$ and $\alpha_2(a)$ are the bending angles (uncorrected) of the signals L1 and L2. This method is known as bending angle correction and is preferred to the first method (Steiner 1998). Using the Abelian transformation (inverse problem), we retrieve the refractive index:

$$\alpha_c(a) = \frac{f_1^2\alpha_1(a) - f_2^2\alpha_2(a)}{f_1^2 - f_2^2} \tag{5}$$

where $a_1 = n(r_t) \times r_t$ is the impact parameter. It is noticed that the integral of the equation needs an infinite upper boundary limit so a background information is used for statistically optimisation the profiles of bending angle. The refractivity based on the parameters of the neutral atmosphere, is given by the formula (Smith and Weintraub 1953) as:

$$\mathrm{N} = (n - 1) \cdot 10^6 = 77.6\frac{P}{T} + 3.73x10^5\frac{e}{T^2} \tag{6}$$

where P is the total atmospheric pressure in [hPa] and T is the atmospheric temperature in [K] and e is the water vapour pressure in [hPa]. To convert the refractivity profiles into pressure and temperature profiles the dry air assumption is usually made. RO observations processing is summarised in the following block diagram (Figure 2).

3. Tropopause heights algorithm

There are many definitions to determine the tropopause location. Among these many definitions of the tropopause, lapse rate tropopause (LRT) is the most common used for measuring climatological variability (Santer et al. 2003). TPH according to the World Meteorological Organization (WMO) definition is defined as 'the lowest level at which the lapse-rate (Γ_{WMO}) decreases to 2 k/km or less, provided that the average lapse-rate between this level (z) and all higher

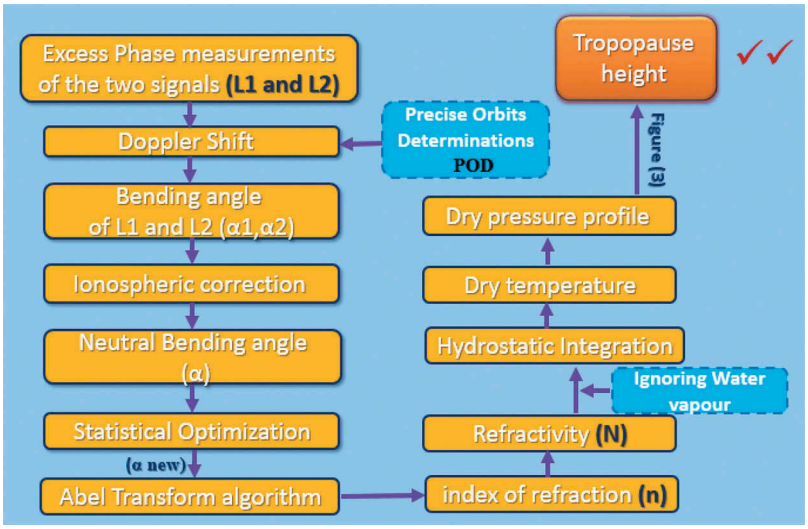

Figure 2. Block diagram for typical RO observations processing.

levels within 2 km above (z +2) does not exceed 2 k/km'. (WMO, 1957)

The ROPP tropopause tool is developed to derive the TPH and tropopause temperature according to four different definitions: A bending angle-based, a refractivity-based and two temperature-based tropopause definitions. The temperature-based tropopause can be derived either from the WMO definition or it can be derived from the cold point definition (ROM SAF Validation Report, 2018). Here, we used the LRT. The LRT is computed by the algorithm described by Reichler et al. (2003). This method uses a thermal definition of the tropopause. For calculating the tropopause temperature, we have to interpolating between vertical levels.

In this research, we calculate the TPH derived from about 2 years of GNSS RO data and compare the results with ECMWF model and heights reported from RS data. The algorithm is summarised in the following block diagram (Figure 3).

4. Data

4.1. MetOp RO data

The location of study area (Egypt) is between the latitudes of 22° and 32° North and longitudes of 25°

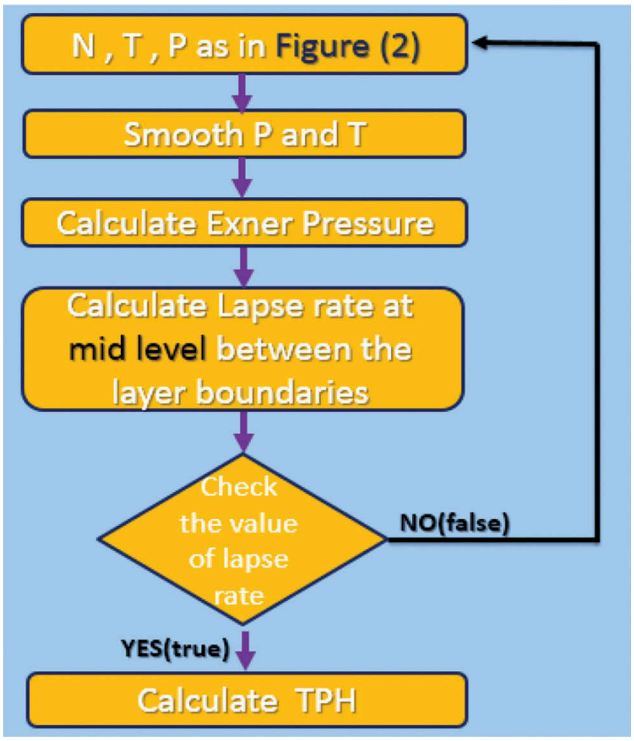

Figure 3. Block diagram for calculating TPH from temperature profile.

and 37° East. For determination the TPH, GNSS RO data provided by the MetOp-A and MetOp-B satellite missions are used. RO profiles including 24 months during the time period spanning from January 2016 to December 2017 of MetOp without any gap (approximately 3597 occultation events). The data are downloaded from the ROMSAF (2016) website (http://www.romsaf.org). Figure 4 shows RO events distribution in 2016 and 2017. Occultations may be either setting or rising based on how LEO see GNSS satellite rises or sets. In Figure 4, The red and blue triangles indicate rising and setting occultations, respectively. From Figure 4, one can understand that the number of occultation events is extremely high and has good coverage over Egypt.

4.2. Radiosonde data

RS data provide atmospheric parameters (such as temperature and pressure profiles). In this study, the RS data were used for validating the GNSS RO results. There are only six RS stations distributed in Egypt. These stations are ASWAN, HELWAN, MERSA MATRUH, FARAFRA, EL ARISH and SOUTH VALLEY UNIV. RS data are downloaded from NOAA (2017) web portal (https://ruc.noaa.gov). Very few data from stations FARAFRA, EL ARISH and SOUTH VALLEY UNIV are available, so we will use only the three other stations (ASWAN, HELWAN and MERSA MATRUH) (Figure 5). A total of 96 profiles of RS observations recorded in Egypt were used to verify the RO technique.

5. Results and discussion

5.1. Analysis of RO TPH

Here, the values of TPH as well as its variation are investigated. TPH is plotted according their latitude in 2016 and 2017 as shown in Figure 6. It is shown from the Figure that generally TPH inversely

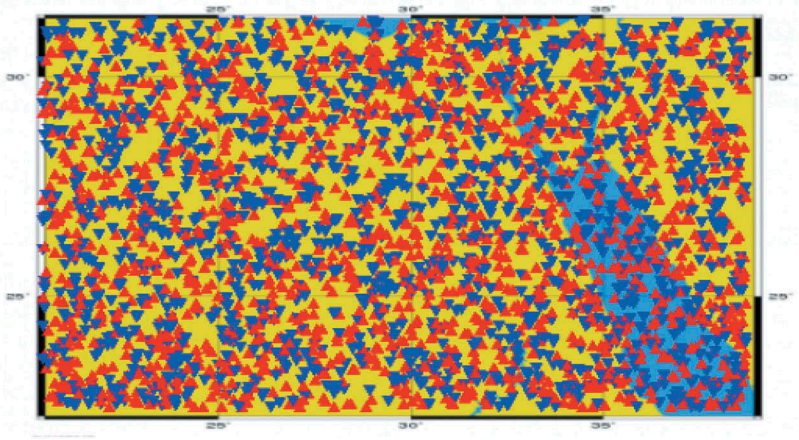

Figure 4. Radio occultation events distribution in 2016 and 2017 over Egypt.

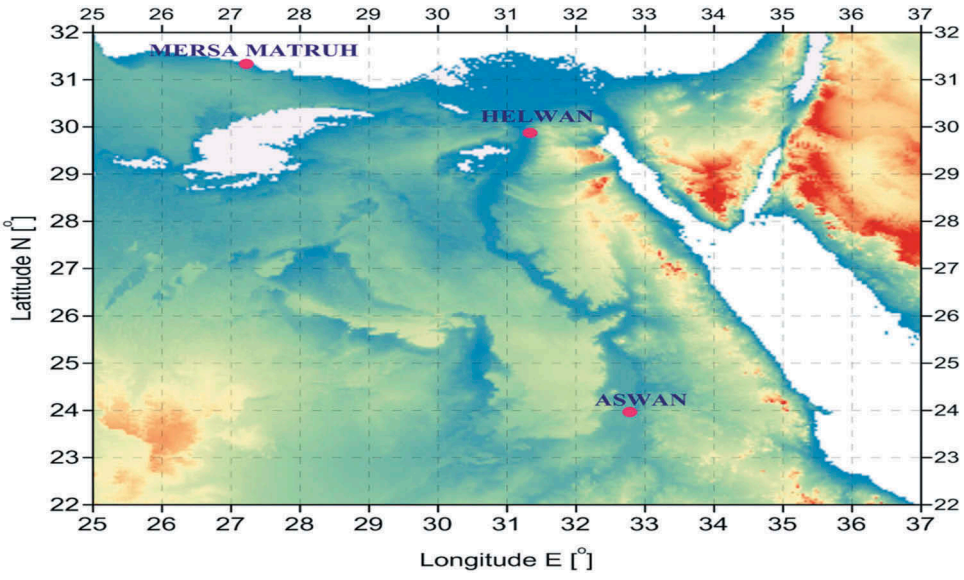

Figure 5. Map of radiosonde stations used in the validation.

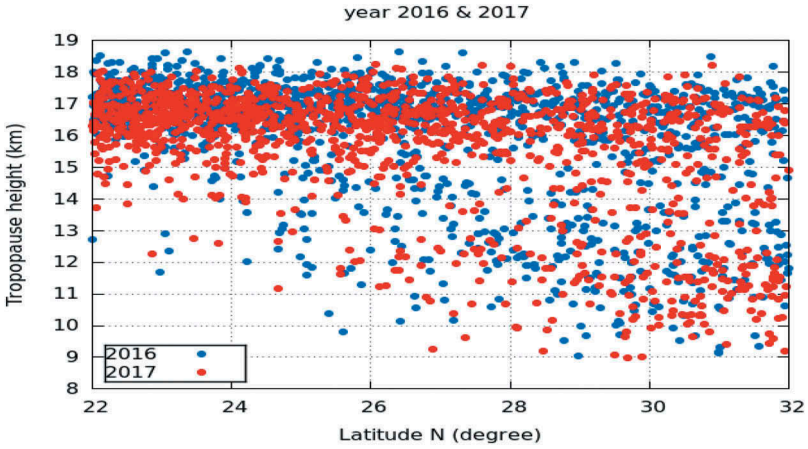

Figure 6. Tropopause height with latitude in 2016 and 2017.

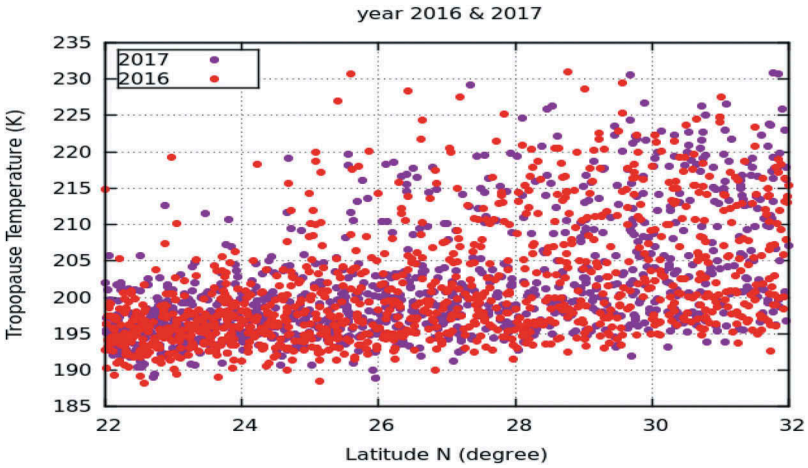

Figure 7. Tropopause temperature with latitude in 2016 and 2017.

correlates with latitude. So, it is obvious that the higher TPH occurs at low latitudes.

Figure 7 shows tropopause temperature estimated from RO data versus latitude in 2016 and 2017 and demonstrates that tropopause temperature increases with latitude so the low TPH (high TPH temperature) occurs at high latitudes.

Generally, tropopause temperature inversely correlates with TPH. So, it is obvious that the higher tropopause temperatures occur at high latitudes. TPH is plotted according to their longitude in 2016 and 2017 as illustrated in Figure 8.

As shown in the previous Figure, it's obvious that TPH shows small variations with longitude.

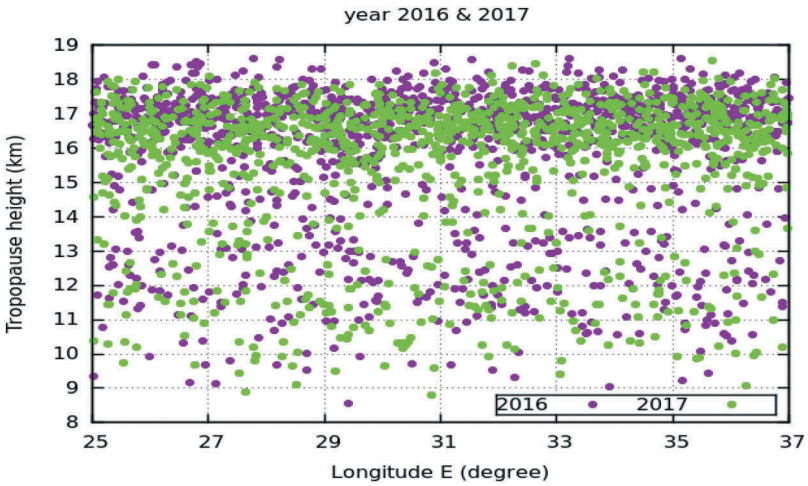

Figure 8. Tropopause height with longitude in 2016 and 2017.

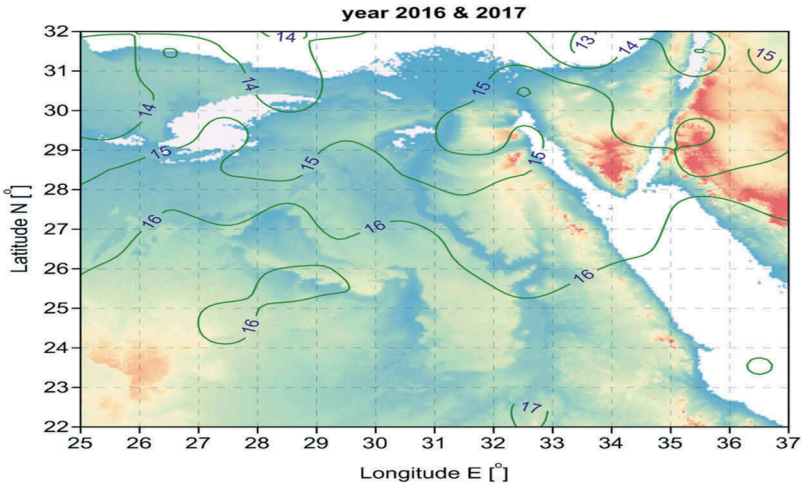

Figure 9. The zonal average tropopause height from the RO data. Units in [Km].

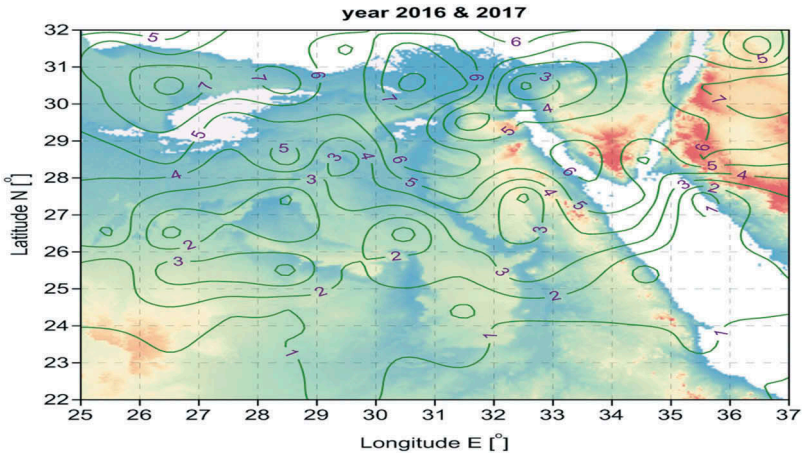

Figure 10. The zonal standard deviation of tropopause height from the RO data. Units in [Km].

The contour maps demonstrating the geographical variation of TPH in 2016 and 2017 is shown in Figure 9. Figure 10 illustrates the zonal standard deviation of TPH from the RO data. Contour plots of tropopause temperature for 2016 and 2017 are shown in Figure 11. The main changing range of TPH is from 14 km to 16 km and it's obvious form the following Figures that TPH decrease with Latitude. Standard deviation here represents scatter around the mean difference.

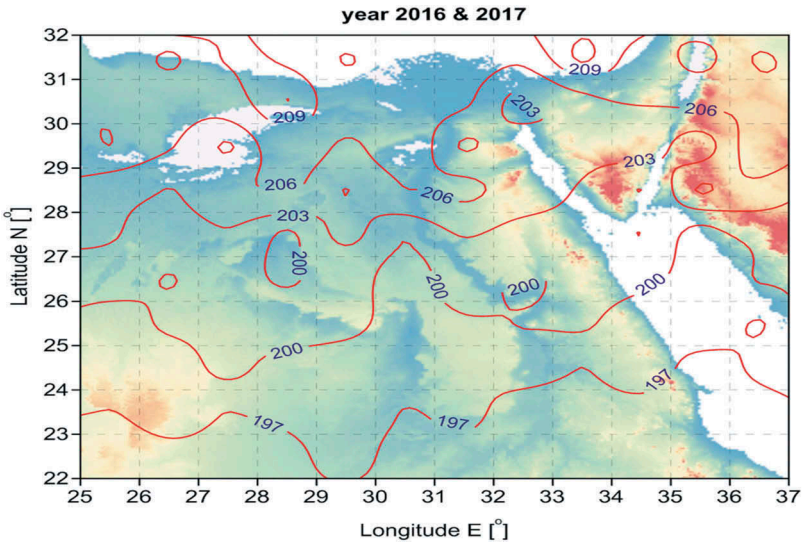

Figure 11. The zonal average tropopause temperature from the RO data. Units in [K].

5.2. Validation the TPH with the background (ECMWF model)

The accuracy of TPH from dry temperature calculated from RO is validated against the tropopause heights estimated from the co-located ECMWF background profiles over the time span January 2016 to December 2017. The TPH is evaluated by estimating the difference between the RO and the *ECMWF* model.

We consider that any difference between the TPH calculated from RO and the ECMWF model greater than 2.5 km as an outlier. The outliers are due to the vertical resolution difference between the RO and ECMWF model. For 2016, the total profiles are 1812 profiles and after deleting the outlier (108 profiles) the remaining profiles become 1704 profiles and this ratio (6%) is not significant. For 2017, the total profiles are 1783 profiles and after deleting the outlier (126 profiles) the remaining profiles become 1657 profiles, and this ratio (7%) is not significant.

Comparison of TPH estimated from RO data and ECMWF model in 2016 and 2017 is shown in Figures 12 and 13.

It is clear from Figures 12 and 13 that there is a good agreement between the results of TPH calculated from RO and ECMWF. The histograms in Figures 14 and 15 indicate a normal distribution nearly with a bias of 0.013 and −0.092 km and with a standard deviation of 0.563 and 0.607 km in 2016 and 2017, respectively.

Figures 16 and 17 illustrate comparison of the tropopause temperature estimated from RO data and ECMWF model in 2016 and 2017, respectively.

As it is clear from the previous Figures there is a good match between the tropopause temperature calculated from RO data and ECMWF model.

5.3. Validation of TPH using radiosonde data

RO TPH is evaluated against TPH calculated from the three RS stations in Egypt. Table 1 gives the coordinates of the three stations. Here, 2016 data are used. The result of the comparison is given in Table 2.

We considered geometric constraint to co-locate RO profiles using Circle of radius 1° Latitude (about 111 km). TPH is evaluated by determining the difference between the RO and the RS stations.

The agreement between calculated TPH from RO and TPH from RS is very good. It goes without saying that RO offer superior spatial and temporal resolution. RO always underestimate

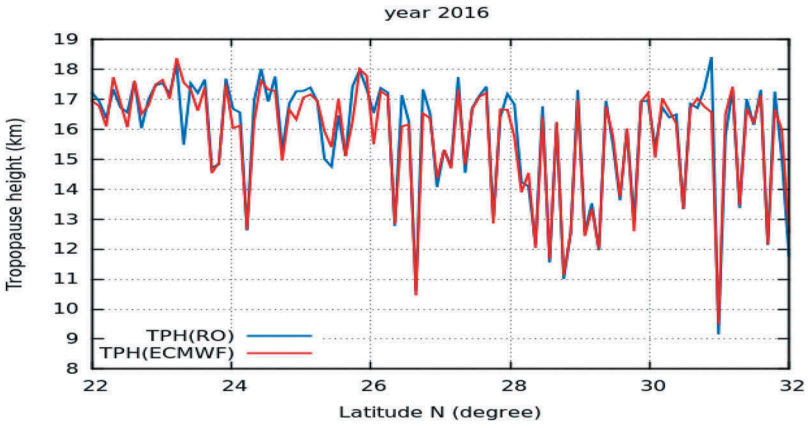

Figure 12. Comparison of tropopause height estimated from RO data and ECMWF model in 2016.

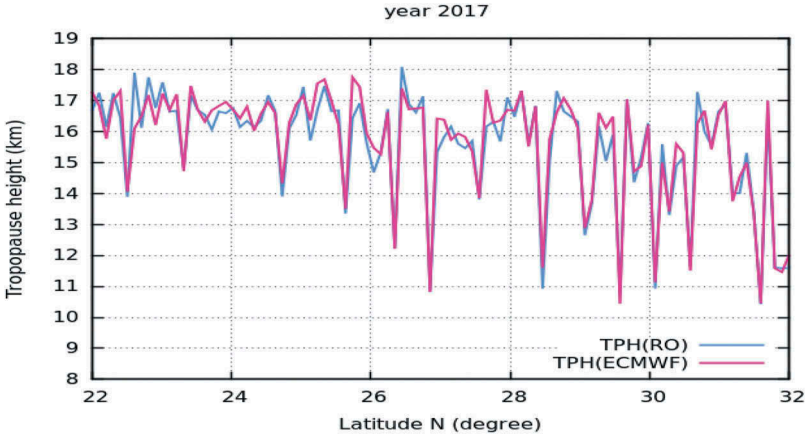

Figure 13. Comparison of tropopause height estimated from RO data and ECMWF model in 2017.

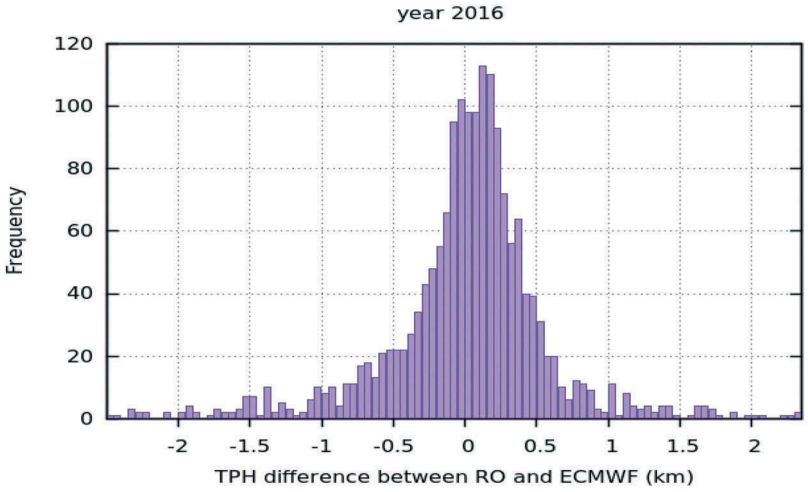

Figure 14. Histogram for tropopause height difference between RO and ECMWF model in 2016.

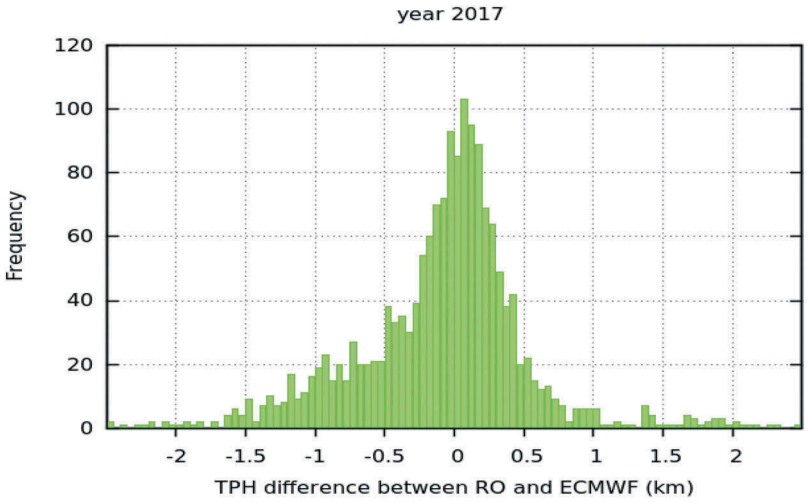

Figure 15. Histogram for tropopause height difference between RO and ECMWF model in 2017.

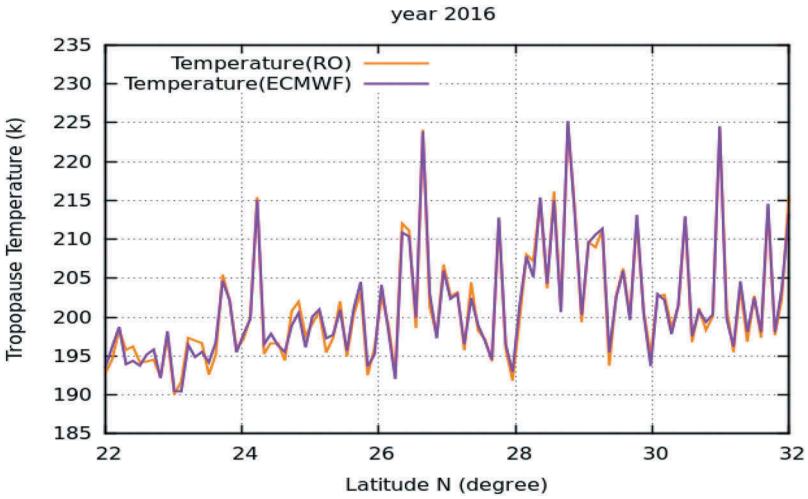

Figure 16. Comparison of tropopause temperature estimated from RO data and ECMWF model in 2016.

TPH for ASWAN and HELWAN while it gives almost perfect match (with RS) at MERSA MATRUH The correlation coefficient was calculated to see how close the relationship is between the RS and the RO derived TPH for selected stations (see Table 2).

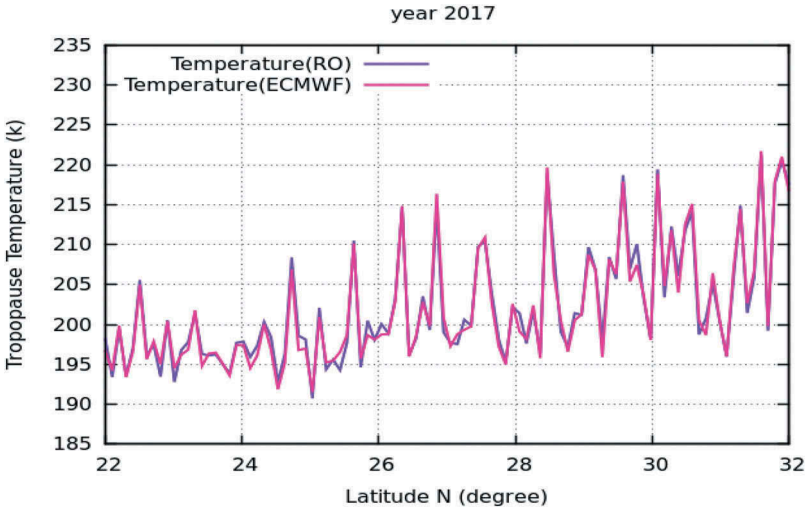

Figure 17. Comparison of tropopause temperature estimated from RO data and ECMWF model in 2017.

Table 1. The used radiosonde stations for validation, including WMO identification number, latitude, longitude and elevation and number of co-located profiles.

Station Name	WMO ID	Lat [°N]	Long [°E]	Elev [m]	No. of co- located profiles
ASWAN	62,414	23.97	32.78	194	20
HELWAN	62,378	29.87	31.33	141	43
MERSA MATRUH	62,306	31.33	27.22	30	33

Table 2. The results of comparison between RO TPH and TPH calculated from the three RS stations.

Station name	Mean difference TPH (km)	Standard deviation (km)	Correlation between RO and RS stations
ASWAN	− 0.6179	0.939	0.899
HELWAN	− 0.179	0.887	0.939
MERSA MATRUH	0.094	0.745	0.945

6. Conclusions

The tropopause height is investigated over Egypt (22° ~32° N, 25°~37° E) based on 3597 occultation profiles covering the period from January 2016 to December 2017. We used the TPH algorithm described by Reichler et al. (2003). The results are validated using ECMWF model and RS data. The validation results show very good agreement with both ECMWF model and RS. For ECMWF model, the mean difference is about −0.092 and 0.013 km for year 2017 and 2016, respectively. The scatter around the mean is about 0.607 and 0.563 km for year 2017 and 2016, respectively.

Analysis of the results shows that RO is a very promising technique for detailed investigation of climate and environmental parameters such as TPH. Analysis of MetOp data show that TPH varies between 14 and 16 km. Generally, TPH decrease with latitude. TPH doesn't show any clear pattern with longitude. The TPH temperature increases with latitude and varies between 197 and 206 K. It is recommended to use more data spanning much longer time to reveals the climate trend of the TPH over Egypt.

Acknowledgments

The authors are grateful to the staff of ROM SAF for providing the data and ROPP software. Dr. Sayed Mekhemer is acknowledged for his fruitful discussions and suggestions. Dr. Torsten Schmidt help and suggestions are highly appreciated. The authors would also like to thank NOAA for the provision of radiosonde data used in this study. Finally, The authors would like to thank the anonymous reviewers for their helpful comments.

Disclosure statement

No potential conflict of interest was reported by the authors.

References

Anthes RA. 2011. Exploring Earth's atmosphere with radio occultation: contributions to weather, climate, and space weather. Atmos Meas Tech. 4:1077–1103. doi:10.5194/amt-4-1077-2011

Anthes RA, Bernhardt PA, Chen Y, Cucurull L, Dymond KF, Ector D, Healy SB, Ho SP, Hunt DC, Kuo Y-H, et al. 2008. The COSMIC/FORMOSAT-3 mission-early results. B Am Meteorol Soc. 89:313–333.

Born M, Wolf. E. 1999. Principles of optics: electromagnetic theory of propagation, interference and diffraction of light. 7th ed. Cambridge (U.K.): Cambridge University Press ; ISBN 0521642221 p. 986 doi:10.2277/0521642221

EUMETSAT ROMSAF Radio Occultation Metrology. 2016. [accessed 2016 May]. http://www.romsaf.org.

Foelsche U. 1999. Tropospheric water vapor imaging by combination of groundbased and spaceborne GNSS sounding data. PhD Thesis. University of Graz (Austria): Institute for Geophysics, Astrophysics, and Meteorology.

Fu E, 2011. An investigation of GNSS radio occultation atmospheric sounding technique for australian meteorology. Ph.D thesis. School of Mathematical and Geospatial Sciences College of Science, Engineering and Health RMIT University.

Fueglistaler S, Dessler AE, Dunkerton TJ, Folkins I, Fu Q, Mote PW. 2009. Tropical tropopause layer. Rev Geophys. 47:RG1004. doi:10.1029/2008RG000267

Hajj GA, Kursinski ER, Romans LJ, Bertiger WI, Leroy SS. 2002. A technical description of atmospheric sounding by GPS occultation, J. Atmos Sol-Terr Phy. 64:451–469.

Holton JR, Haynes PH, McIntyre ME, Douglass AR, Rood RB, Pfister L. 1995. Stratosphere-troposphere exchange. Rev Geophys. 33:403–440.

Kirchengast G, Schweitzer S, Schwaerz M, Fritzer J, Gorbunov M. 2006. Advanced retrieval processing chain for derivation of atmospheric profiles from LEO LEO radio occultation data). Technical Report for ESA/ESTEC No. 2/2006. Institute for Geophysics, Astrophysics, and Meteorology.

Kursinski ER, Hajj GA, Hardy KR, Schofield JT, Linfield R. 1997. Observing earth's atmosphere with radio occultation measurements, J. Geophys Res. 102:23429–23465.

NOAA Research. 2017. [accessed Jan 2017]. https://ruc.noaa.gov.

Randel WJ, Park M, Wu F, Livesey N. 2007. A large annual cycle in ozone above the tropical tropopause linked to the Brewer-Dobson circulation. J Atmos Sci. 64(12):4479–4488.

Reichler T, Dameris M, Sausen R. 2003. Determination of tropopause height from gridded data, Geophys. Res Lett. 30(20):2042. doi:10.1029/2003GL018240.

ROM SAF. 2018. Validation report: reprocessed Level 2C tropopause height CDR v1.0 products. SAF/ROM/DMI.

Santer BD, Sausen R, Wigley TML, Boyle JS, AchutaRao K, Doutriaux C, Hansen JE. 2003. Behavior of tropopause height and atmospheric temperature in models, reanalyses, and observations: decadal changes. J Geophys Res. 108:ACL1–1-1-22. doi:10.1029/2002JD002258

Smith E, Weintraub S, 1953. The constants in the equation for atmospheric refractive index at radio frequencies. Proceedings of the IRE 41, pp. 1035–1037.

Steiner A, Lackner B, Ladstädter F, Scherllin-Pirscher B, Foelsche U, Kirchengast G. 2011. GPS radio occultation for climate monitoring and change detection. Radio Sci. 46:RS0D24. doi:10.1029/2010RS004614

Steiner AK, 1998. High resolution sounding of key climate variables using the radio occultation technique. PhD thesis. University of Graz, Austria: Institute for Geophysics, Astrophysics, and Meteorology.

Vorob'ev VV, Krasil'nikova TG. 1994. Estimation of the accuracy of the atmospheric refractive index recovery from Doppler shift measurements at frequencies used in the NAVSTAR system. Phys Atmos Ocean. 29:602–609.

Ware R, Exner M, Feng D, Gorbunov M, Hardy K, Herman B, Kuo Y, Meehan T, Melbourne W, Rocken C, et al. 1996. GPS sounding of the atmosphere from low earth orbit: preliminary results. B Am Meteorol Soc. 77:19–40.

World Meteorological Organization (WMO), 1957. Definition of the tropopause, WMO Bulletin 6, Geneva (Switzerland).